MECSOL 2022 - Proceedings of the 8th International Symposium on Solid Mechanics
M.L. Bittencourt, J. Labaki, L.C.M. Vieira Jr. and E. Mesquita (Editors), Campinas SP, Brazil, October 17th to 19th, 2022

STABILITY AND DYNAMIC BEHAVIOR OF A CANTILEVERED VISCOELASTIC PIPE ASPIRATING INTERNAL FLUID

Jorge David Apaza [1], Lenin Lee Valdivia [1], Juan Pablo Avila [1]

[1] Federal University of ABC, São Paulo, Av. dos Estados, 5001, Brazil

Abstract: *The present study, analyzes the stability and dynamic behavior of a cantilevered viscoelastic pipe disposed vertically and aspirating internal fluid. The structural model is based on the Euler-Bernoulli beam theory, the internal flow is of the type plug-flow. The dynamic equation is derived by Newtonian method, it was observed that the Coriolis force for aspirating is unstable, different from the case of discharge that behaves as a stabilizer, this generated an increase in the start of instability. The force acting on the free end of the pipe due to depressurization of the fluid being aspirated is considered, which is transmitted axially along the pipe. The differential govern equation of the system was discretized by the Galerkin method. The natural frequencies have been calculated for different internal flow velocity and the results obtained are presented in the Argand diagram where it is possible to identify the critical flow velocity. The system loss stability due first-mode due to unique type via Hopf bifurcation by flutter at small velocity flow values. The numerical analysis of the system to calculate the stable-state response, is carried, the system is exited harmonic force in the time domain. The dynamic response of the system is obtained out through the Laplace transformation method. to its boundary conditions, the force acting on the free end caused by the aspirating, has a great effect on the deformation of the pipe. In general, the results show a loss by first-mode stability due to flutter, which are consistent with the results available in the literature, observing a good coherence of the results.*

Keywords: Pipe aspirating fluid; stability; dynamic; Galerkin method.

INTRODUCTION

Fluid aspirating pipes have different applications in engineering, such as in the extraction of minerals in the deep ocean, and the sea water is aspirating in by ships, it is used to cool the processes on the platform. The need arises to understand stability and the dynamic behavior of this type of structure for different internal fluid velocities, since there is a critical velocity above which the system becomes unstable. This problem has motivated Paidoussis & Luu (1985) to conduct an analytical study, on this subject were by replacing $+U$ with $-U$ in the linear equation of motion for a cantilevered pipe discharging fluid, concluded that the aspirating pipe loses stability by flutter at low flow velocities.

After more than a decade, Paidoussis (1999) carried out experiments in order to revalidate its previously obtained analytical results, concluding that the flow at the pipe inlet is not like discharge case, i.e., the fluid does not inlet in the pipe as a reverse jet, rather, flow enters similar to a sink. The sudden increase of the velocity induces a depressurization at the inlet. Subsequently, Paidoussis et al. (2005) performed a new theoretical revision of the problem. Instead, then a sink flow, exist a mean flow velocity just in front of the inlet, at the beginning the fluid particle is far from the pipe inlet with zero velocity, the particle was accelerated until it reaches a velocity around the pipe inlet, and is greater than the velocity inside the pipe. Also, the author considers a compressive force on the lip of the pipe, due to flow when aspirating.

Michael P. Paidoussis (2005) obtained more comprehensive results on this topic, the main of them is the inlet velocity remains tangential to the free end of the pipe. In addition, the pipe can be subjected to flutter, this depending on the inlet velocity and the angle of inclination of the pipe. Rinald (2009) and Giacobbi et al. (2012) giving continuity to the work of Paidoussis et al. (2005), performed numerical simulations by CFD, in order to understand the interaction between the free end of the pipe and aspired flow, identifying values of important parameters that model the forces acting on the free end of the pipe.

Recently, multinational oil and gas company Shell start to use suspended pipes of viscoelastic material, also known as Water Intake Riser (WIR), where water is aspirating into ship platform to cooling process by Minguez et al., (2020). Another example of its use is in OTEC power plants (Ocean Thermal Energy Conversion). Currently, many researchers agree that in the sea to the northeast of Brazil has the potential to install OTEC plants by Rodrigo Klim, (2021). Here the following questions arise: Can WIR become unstable due to fluid aspiration? and, at what velocity could this happen? these questions are addressed in this article.

This work has as objectives, (1) perform a numerical study of the stability of a pipe aspirating internal fluid; (2) simulate the dynamic behavior of the same pipes subjected to harmonic excitation. The structure of this work is as follows,

initially the mathematical model is presented, then the Galerkin method is applied to discretize the government equation. The complex natural eigenfrequencies are presented in the Argand diagram to analyze the stability of the system, follow the response of the system is subjected to a harmonic excitation is presented for a fluid velocity of interest. Finally, follows the conclusions of this work.

EQUATION OF MOTIONS

The Fig. 1(a) show schematic of a pipe aspirating internal fluid, basing on the complete development the equations of motion by Michael P. Paidoussis (2005). The same is disposed vertically and seen as a cantilever beam, where the fluid is being aspirated by the free end. For its analysis, the following hypotheses are adopted. 1) The length of the pipe is greater than its diameter, and lateral motions $w(x,t)$ small compared to the diameter, pipe is subjected to small lateral deflections and consequently small rotations θ, is slender, so the beam theory of Euler-Bernoulli is assumed. 2) The pipe is considered to be inextensible. 3) The internal flow is steady, uniform, similar to a plug-flow, and of constant axial velocity U. 4) The pipe material is subjected to internal dissipation of the Kelvin-Voigt type. 5) The rotary shear deformation, friction and inertial rotation, as well as external forces are omitted. 6) A two-dimensional analysis is considered in the x-z plane.

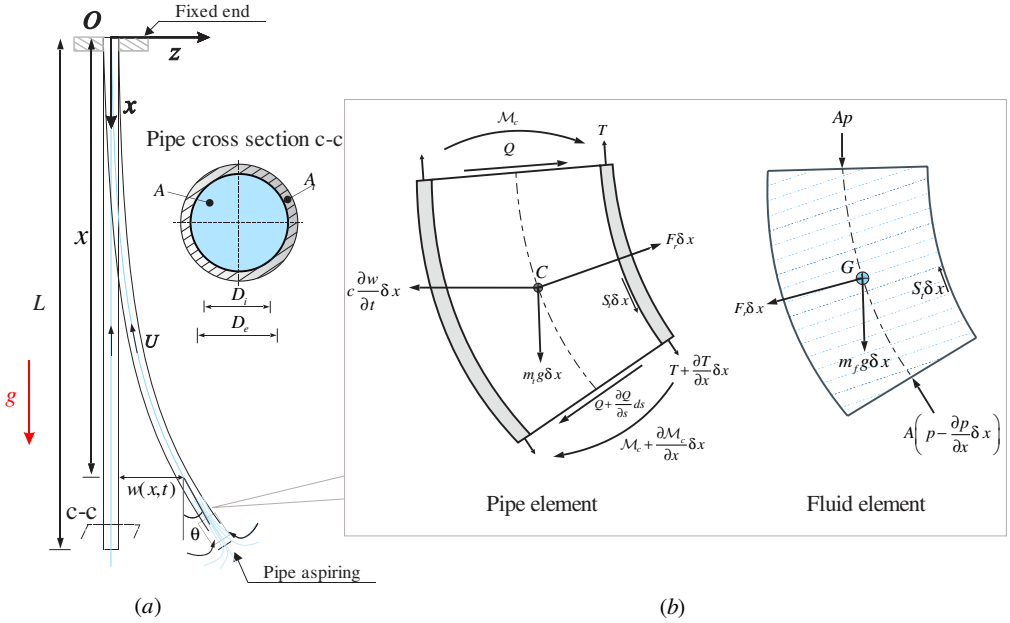

Figure 1 – Schematic representation: (a) A cantilevered pipe aspirating fluid; (b) Fluid-structure forces acting on an element of length δx of the cantilevered pipe.

The plug-flow has cross-sectional area A and mass per unit length of fluid m_f. Consider the fluid element, as seen in Fig 1 (b). Assuming a small deflection and rotations, the equation of motion will be obtained using Newton's second law in the two directions as follows,

$$\sum F_x = 0, \qquad A\frac{\partial p}{\partial x} - S_t + m_f g + F_r\frac{\partial w}{\partial x} = 0 \tag{1}$$

$$\sum F_z = 0, \qquad F_r - A\frac{\partial}{\partial x}\left(p\frac{\partial w}{\partial x}\right) + S_t\frac{\partial w}{\partial x} + m_f\left(\frac{\partial w}{\partial t} - U\frac{\partial w}{\partial x}\right)^2 = 0 \tag{2}$$

where S_t is the shear stress on the internal surface of the pipe multiplied by its perimeter, p is the internal pressure acting on a fluid element, F_r is the radial force per unit length imposed by the fluid element to the pipe.

Figure 2 also shows the forces acting on a pipe element. Applying Newton's second law in the x and z directions, gives,

$$\sum F_x = 0, \qquad \frac{\partial T}{\partial x} + S_t + m_t g + F_r\frac{\partial w}{\partial x} = 0 \tag{3}$$

$$\sum F_z = 0, \qquad \frac{\partial Q}{\partial x} + F_r + \frac{\partial}{\partial x}\left(T\frac{\partial w}{\partial x}\right) + S_t\frac{\partial w}{\partial x} - c\frac{\partial w}{\partial x} - m_t\frac{\partial^2 w}{\partial x^2} = 0 \tag{4}$$

where m_f is mass per unit length of pipe, c is the viscous damping coefficient, Q is the lateral shear force, T is the axial tension.

The elementary theory of beam applies to moments at the center of the pipe element, the moment-curvature relationship is,

$$Q = -\frac{\partial \mathcal{M}_c}{\partial x} = -EI\left[1 + \left(\bar{\alpha} + \frac{\mu}{\Omega}\right)\frac{\partial}{\partial t}\right]\frac{\partial^3 w}{\partial x^3} \tag{5}$$

where EI is the flexural rigidity, $\mathcal{M}_c$ is the bending moment, $\bar{\alpha}$ is the Kelvin-Voight viscoelastic damping coefficient, μ is the hysteretic damping coefficient and Ω is the circular frequency of oscillation, Paidoussis and Des Trois Maisons, (1971) were the ones that studied the effect of material damping on the dynamics of a transport fluid of a vertical cantilever pipe.

The governing equation freely hanging pipe and aspirating fluid, have been defined, combining forces acting in the x direction, Eq. (1) (3) and (5) are used and gives,

$$EI\left[1 + \left(\bar{\alpha} + \frac{\mu}{\Omega}\right)\frac{\partial}{\partial t}\right]\frac{\partial^4 w}{\partial x^4} - \frac{\partial}{\partial x}\left((T - pA)\frac{\partial w}{\partial x}\right) - 2m_f U\frac{\partial^2 w}{\partial x \partial t} + MU^2\frac{\partial^2 w}{\partial x^2} + c\frac{\partial w}{\partial t} + \left(m_t + m_f\right)\frac{\partial^2 w}{\partial t^2} = 0 \tag{6}$$

Similarly, forces acting in the y direction Eq. (2) in Eq. (4) are combined to give,

$$\frac{\partial}{\partial x}(T - pA) = -\left(m_t + m_f\right)g \tag{7}$$

and integrating Eq. (7) from x to L.

$$(T - pA)|_{x=L} = (\bar{T} - \bar{p}A) - \left(m_t + m_f\right)g(L - x) \tag{8}$$

where $\bar{T}$ is the axial force exerted on the lip of the pipe and $\bar{p}A$ is the depressurization force produced by aspirating fluid.

Forces acting on the pipe inlet

Figure 2 (a) shows the fluid particles flow entering the mouth of the pipe with velocity V_e, whose direction forms an angle χ with the x-axis. The fluid particles achieve a uniform flow velocity U, θ_L is the angle of rotation of the free end of the pipe. In Fig. 2 (b) show the inlet velocity components V_e , and at the outlet velocity inside U, and the transverse velocity of the free end of the pipe $\dot{w}_L$. In Fig. 2(c) shows the pressure loss components in x-z directions, this pressure is due to the flow acceleration and is evaluated using the Bernoulli equation, applied when the velocity increases from about 0 to U, and becomes $p_{loss} = 1/2\, m_f U^2$.

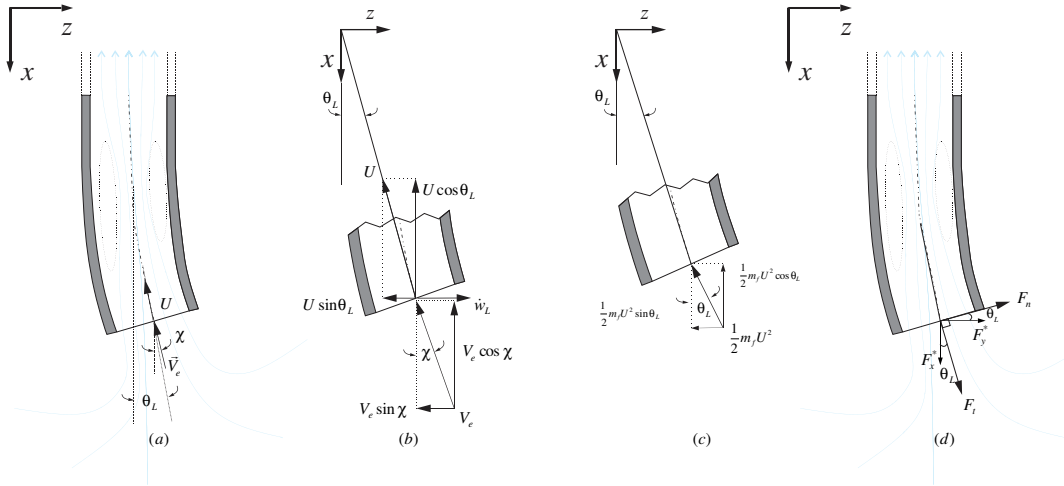

Figure 2 – Schematic representation the free end of the pipe: (a) definition of the angles and velocities; (b) components of velocities; (c) components of forces due to depressurization; (d) forces exerted by the fluid on the pipe

The forces exerted by the pipe on the fluid is equal to the change rate of the momentum of fluid particles entering in pipe. The components of these forces in the x and y directions are given by, $F_x = MU\left(V_{oulet,x} - V_{inlet,x}\right) + p_{loss,x}$ and $F_x = MU\left(V_{oulet,y} - V_{inlet,y}\right) + p_{loss,y}$, expressed as,

$$F_x = m_f U[(-U\cos\theta_L) - (-V_e\cos\chi)] - \frac{1}{2}m_f U^2\cos\theta_L \tag{9}$$

$$F_y = m_f U[(\dot{w}_L - U\sin\theta_L) - (-V_e\sin\chi)] - \frac{1}{2}m_f U^2\sin\theta_L \tag{10}$$

Assuming small deflections angle, θ_L, approximate to $\cos\theta_L \approx \cos\chi \approx 1$, $\sin\theta_L \approx \theta_L \approx w_L'$ and presumed the fluid velocity vector forms the with the vertical is $\sin\chi \approx \chi = \kappa\theta_L$.

Furthermore, assuming the approximations, thus, Eq. (9) and (10) is simplify,

$$F_x = -m_f U^2 \left[\frac{3}{2} - \alpha\right] \tag{11}$$

$$F_y = m_f U \dot{w}_L - m_f U^2 w_L' \left(\frac{3}{2} - \alpha\kappa\right) \tag{12}$$

where the parameter $\alpha = V_e/U$ is the velocity ratio near to the inlet and inside the pipe, and κ is a reduction angle factor indicating that the inlet is not purely tangential.

Finally, the forces exerted by the fluid flow on the pipe, F_x^* and F_y^*, as seen in Fig. 2 (d), are obtained by changing the sign of Equations (11) and (12), ($F_x^* = -F_x$) and ($F_y^* = -F_y$). Such forces are expressed in the normal and tangential coordinate system, being the normal component F_n and tangential F_t, and give,

$$F_t \approx F_x^* \tag{13}$$

$$F_n \approx F_x^* - F_y^* = -m_f U[\dot{w}_L - U\alpha(1-\kappa)w_L'] \tag{14}$$

Supposed that, the depressurization force at the inlet is equal to the tangential force by the fluid on the pipe at the inlet, expressed as,

$$-\bar{p}A = F_t = m_f U^2 \left[\frac{3}{2} - \alpha\right] \tag{15}$$

Then, CFD analysis carried out by Giacobbi et al. (2012) confirmed the existence of a pressure on the lip of the pipe related to depressurization at the inlet, resulting in the tension $\bar{T}$ in the pipe, and is expressed as

$$\bar{T} = -\Upsilon\zeta\bar{p}(A_t - A) = -\bar{\gamma} m_f U^2 \left[\frac{3}{2} - \alpha\right] \tag{16}$$

where Υ is the pressure ratio at the pipe inlet and the pipe lip, ζ is area ratio $\zeta = (A_t - A)/A$, with values between ($0 < \zeta < 1$), A_t and A are the cross-sectional areas of the pipe and the plug-flow, $\bar{\gamma}$ is the ratio of tension at the free end of the pipe, $\bar{\gamma} = \zeta\Upsilon$.

Consequently, the axial force is obtained by substituting Eq. (15) and (16) in Eq. (8) can be expressed as.

$$\bar{T} - \bar{p}A = -m_f U^2(1+\bar{\gamma})\left(\frac{3}{2} - \alpha\right) \tag{17}$$

Boundary conditions

The pipe object of study has the following boundary conditions. Since in top is fixed, so the deflection and rotation are zero and the free, therefore, there is no bending moment and the shear force in the lateral direction, is equal to F_n given by Eq (14). Mathematically, it is obtained,

$$x = 0 \qquad w(0,t) = 0 \quad , \qquad \frac{\partial w(0,t)}{\partial x} = 0 \tag{18}$$

$$x = L \qquad EI\frac{\partial^2 w(L,t)}{\partial x^2} = 0 \quad , \qquad EI\frac{\partial^3 w(L,t)}{\partial x^3} = -m_f U\left(\frac{\partial w(L,t)}{\partial t} - U\alpha(1-\kappa)\frac{\partial w(L,t)}{\partial x}\right) \tag{19}$$

Final expression of the equation of motion

The equation of motion for the pipe, obtained by substituting the Eq. (17) and (19) into Equation (6), gives,

$$\begin{aligned} EI\left[1 + \left(\tilde{\alpha} + \frac{\mu}{\Omega}\right)\frac{\partial}{\partial t}\right]\frac{\partial^4 w}{\partial x^4} + \left(1 - (\bar{\gamma}+1)\left(\frac{3}{2} - \alpha\right) - \left(m_f + m_t\right)g(L-x)\right)m_f U^2\frac{\partial^2 w}{\partial x^2} - 2m_f U\frac{\partial^2 w}{\partial x \partial t} + c\frac{\partial w}{\partial t} \\ + \left(m_f + m_t\right) + g\frac{\partial w}{\partial x} + \left(m_t + m_f\right)\frac{\partial^2 w}{\partial t^2} + m_f U\left(\frac{\partial w}{\partial t} - U\alpha(1-\kappa)\frac{\partial w}{\partial x}\right)\delta(x-L) = 0 \end{aligned} \tag{20}$$

where shear force is the last term of Eq. (20) and is introduced through the Dirac delta function, $\delta(x-L)$.

The motion Equation (20) is non-dimensionalized with the following dimensionless parameters, which are defined as,

$$\begin{aligned} \xi = \frac{x}{L}, \quad \eta = \frac{w}{L}, \quad \tau = \left(\frac{EI}{\left(m_f + m_t\right)L^4}\right)^{\frac{1}{2}} t, \quad \omega = \left(\frac{\left(m_f + m_t\right)L^4}{EI}\right)^{\frac{1}{2}}\Omega, \quad u = UL\left(\frac{m_f}{EI}\right)^{\frac{1}{2}}, \gamma \\ = \frac{\left(m_f + m_t\right)gL^3}{EI}, \beta = \frac{m_f}{m_f + m_t}, \quad \tilde{\alpha}^* = \left(\frac{EI}{\left(m_f + m_t\right)L^4}\right)^{\frac{1}{2}}\tilde{\alpha}, \quad \sigma = \frac{cL^2}{\left[EI\left(m_f + m_t\right)\right]^{\frac{1}{2}}} \end{aligned} \tag{21}$$

where ξ is dimensionless longitudinal coordinate, η is dimensionless displacement, ω is dimensionless circular frequency of oscillation, u is dimensionless flow velocity, β is dimensionless mass parameter, and $\bar{\alpha}^*$ is dimensionless viscoelastic dissipation, γ is dimensionless weight of the system, and σ is dimensionless viscous damping due to the surrounding fluid.

The system's equation of motion, Eq. (20), is expressed in dimensionless form using the aforementioned quantities, Eq. (21), getting,

$$\left[1+\left(\bar{\alpha}^*+\frac{\mu}{\omega}\right)\frac{\partial}{\partial\tau}\right]\frac{\partial^4\eta}{\partial\xi^4}+\left(\left(1-(\bar{\gamma}+1)\left(\frac{3}{2}-\alpha\right)\right)u^2-\gamma(1-\xi)\right)\frac{\partial^2\eta}{\partial\xi^2}-2\beta^{\frac{1}{2}}u\frac{\partial^2\eta}{\partial\xi\partial\tau}+\sigma\frac{\partial\eta}{\partial\tau}+\gamma\frac{\partial\eta}{\partial\xi}+\frac{\partial^2\eta}{\partial\tau^2}+\left(\beta^{\frac{1}{2}}u\frac{\partial\eta}{\partial\tau}-u^2\alpha(1-\kappa)\frac{\partial\eta}{\partial\xi}\right)\delta(\xi-1)=0 \tag{22}$$

DISCRETIZATION OF THE MATHEMATICAL MODEL

The Eq. (22) is discretized using Galerkin's method, considering that the solution is the sum of the products of a spatial and temporal function,

$$\eta(\xi,\tau)=\sum_{j=1}^{N}\varphi_j(\xi)q_j(\tau) \tag{23}$$

where $\varphi_j(\xi)$ is the dimensionless "j" comparison function of a cantilevered pipe, and $q_j(\tau)$ is the "j" generalized coordinate of the discretized system, N is a high integer of assumed mode shapes.

Additionally, comparison the function $\varphi_j(\xi)$ satisfies the orthogonality propriety, $\varphi_j{}''''(\xi)=\lambda^4\varphi_j(\xi)$, where λ is the eigenvalue, these values in the modal function are approached as the eigenfunctions of the cantilever beam and satisfy the boundary condition of the systems.

The govern equation is discretized using Galerkin's method, substituting Eq. (23) in Eq. (22), to obtain,

$$\sum_{j=1}^{N}\left[\lambda^4\varphi_j(\xi)q_j(\tau)+\lambda^4\left(\bar{\alpha}^*+\frac{\mu}{\omega}\right)\varphi_j(\xi)\dot{q}_j(\tau)+\left(\left(1-(\bar{\gamma}+1)\left(\frac{3}{2}-\alpha\right)\right)u^2-\gamma(1-\xi)\right)\varphi_j{}''(\xi)q_j(\tau)-2\beta^{\frac{1}{2}}u\varphi_j{}'(\xi)\dot{q}_j(\tau)+\sigma\varphi_j(\xi)\dot{q}_j(\tau)+\gamma\varphi_j{}'(\xi)q_j(\tau)+\varphi_j(\xi)\ddot{q}_j(\tau)+\delta(\xi-1)\left(\beta^{\frac{1}{2}}u\varphi_j(\xi)\dot{q}_j(\tau)-u^2\alpha(1-\kappa)\varphi_j{}'(\xi)q_j(\tau)\right)\right]=\varepsilon_N \tag{24}$$

where the approximate solution produces a non-zero residual due to sum, ε_N.

In order for the residual to approach zero, the weighting function is applied in Galerkin's method, the statement of the integral by Reddy (2002) follows,

$$\int_0^1\varphi_i(\xi).\,\varepsilon_N d\xi=0 \tag{25}$$

where $\varphi_i(\xi)$ is the dimensionless "i" weighting function and seen as can be taken as the known cantilevered beam eigenfunctions, with the domain of integration from 0 to 1. Applying Eq. (25) in Eq. (24) are obtained,

$$\sum_{j=1}^{N}\left[\lambda_j^4\left(\int_0^1\varphi_i(\xi)\varphi_j(\xi)d\xi\right)q_j(\tau)+\lambda_j^4\left(\bar{\alpha}^*+\frac{\mu}{\omega}\right)\left(\int_0^1\varphi_i(\xi)\varphi_j(\xi)d\xi\right)\dot{q}_j(\tau)+\left(\left(1-(\bar{\gamma}+1)\left(\frac{3}{2}-\alpha\right)\right)u^2-\gamma\right)\left(\int_0^1\varphi_i(\xi)\varphi_j{}''(\xi)d\xi\right)q_j(\tau)+\gamma\left(\int_0^1\varphi_i(\xi)\varphi_j{}''(\xi)\xi d\xi\right)q_j(\tau)-2\beta^{\frac{1}{2}}u\left(\int_0^1\varphi_i(\xi)\varphi_j{}'(\xi)d\xi\right)\dot{q}_j(\tau)+\sigma\left(\int_0^1\varphi_i(\xi)\varphi_j(\xi)d\xi\right)\dot{q}_j(\tau)+\gamma\left(\int_0^1\varphi_i(\xi)\varphi_j{}'(\xi)d\xi\right)q_j(\tau)+\left(\int_0^1\varphi_i(\xi)\varphi_j(\xi)d\xi\right)\ddot{q}_j(\tau)+\beta^{\frac{1}{2}}u\left(\int_0^1\varphi_i(\xi)\varphi_j(\xi)\delta(\xi-1)d\xi\right)\dot{q}_j(\tau)-u^2\alpha(1-\kappa)\left(\int_0^1\varphi_i(\xi)\varphi_j{}'(\xi)\delta(\xi-1)d\xi\right)q_j(\tau)=\int_0^1\varphi_i(\xi).\,\varepsilon_N d\xi \tag{26}$$

The following sets of coefficients are defined,

$$\delta_{ij} = \int_0^1 \varphi_i(\xi)\varphi_j(\xi)d\xi\,, \quad b_{ij} = \int_0^1 \varphi_i(\xi)\varphi_j{}'(\xi)d\xi,$$
$$c_{ij} = \int_0^1 \varphi_i(\xi)\varphi_j{}''(\xi)d\xi\,, \quad d_{ij} = \int_0^1 \varphi_i(\xi)\varphi_j{}''(\xi)\xi d\xi \tag{27}$$

The numerical values of the integrals of Eq. (27) are found in Appendix B of Paidoussis (1998).

$$\sum_{j=1}^{N}\Bigg[\lambda_j^4\delta_{ij}q_j(\tau) + \lambda_j^4\left(\bar{\alpha}^* + \frac{\mu}{\omega}\right)\delta_{ij}\dot{q}_j(\tau) + \left(\left(1-(\bar{\gamma}+1)\left(\frac{3}{2}-\alpha\right)\right)u^2-\gamma\right)c_{ij}q_j(\tau) + \gamma d_{ij}q_j(\tau)$$
$$-2\beta^{\frac{1}{2}}ub_{ij}\dot{q}_j(\tau) + \sigma\delta_{ij}\dot{q}_j(\tau) + \gamma b_{ij}q_j(\tau) + \delta_{ij}\ddot{q}_j(\tau)$$
$$+\beta^{\frac{1}{2}}u\phi_i(1)\varphi_j(1)\dot{q}_j(\tau) - u^2\alpha(1-\kappa)\phi_i(1)\varphi_j{}'(1)q_j(\tau)\Bigg] = 0 \qquad i = 1,2,3,\dots,N; \tag{28}$$

The set of discretized equations, Eq. (28), is grouped and expressed in matrix form in function of the generalized coordinates $q_j(\tau)$, which leads to an expression of the form.

$$[M]\{\ddot{q}(\tau)\} + [C]\{\dot{q}(\tau)\} + [K]\{q(\tau)\} = 0 \tag{29}$$

where $[M]$, $[C]$, and $[K]$ are the mass, dissipation, and stiffness matrices, and we can write the elements of the matrices as,

$$M_{ij} = \delta_{ij} \tag{30}$$

$$C_{ij} = \left(\left(\bar{\alpha}^* + \frac{\mu}{\omega}\right)\lambda_j^4 + \sigma\right)\delta_{ij} - 2\beta^{\frac{1}{2}}ub_{ij} + \beta^{\frac{1}{2}}u\varphi_i(1)\varphi_j(1) \tag{31}$$

$$K_{ij} = \lambda_j^4\delta_{ij} + \gamma b_{ij} + \left(\left(1-(\bar{\gamma}+1)\left(\frac{3}{2}-\alpha\right)\right)u^2-\gamma\right)c_{ij} + \gamma d_{ij} - \alpha(1-\kappa)u^2\varphi_i(1)\varphi_j{}'(1) \tag{32}$$

Eigenvalue analysis

The discretized equations of motion, Eq. (29), is used to calculate the eigenvalues of the pipe aspirating internal fluid,

$$[\delta_{ij}]\{\ddot{q}_j(\tau)\} + \left[\left(\left(\bar{\alpha}^* + \frac{\mu}{\omega}\right)\lambda_j^4 + \sigma\right)\delta_{ij} - 2\beta^{\frac{1}{2}}ub_{ij} + \beta^{\frac{1}{2}}u\varphi_i(1)\varphi_j(1)\right]\{\dot{q}_j(\tau)\}$$
$$+\left[\lambda_j^4\delta_{ij} + \gamma b_{ij} + \left(\left(1-(\bar{\gamma}+1)\left(\frac{3}{2}-\alpha\right)\right)u^2-\gamma\right)c_{ij} + \gamma d_{ij} - \alpha(1-\kappa)u^2\varphi_i(1)\varphi_j{}'(1)\right]\{q_j(\tau)\} = 0 \tag{33}$$

The solution of Eq. (33) is assumed to have the form of $\{q_j(\tau)\} = \{q_j\}e^{-i\omega\tau}$ where "i" is the imaginary unit number and ω is the circular dimensionless frequency. Substituting the assumed solution into Eq. (33) and obtain.

$$\Bigg[-\omega^2\delta_{ij} + \left(\left(\bar{\alpha}^* + \frac{\mu}{\omega}\right)\lambda_j^4 + \sigma\right)\delta_{ij} - \left(2\beta^{\frac{1}{2}}ub_{ij} - \beta^{\frac{1}{2}}u\varphi_i(1)\varphi_j(1)\right)i\omega + \lambda_j^4\delta_{ij} + \gamma b_{ij}$$
$$+\left(\left(1-(\bar{\gamma}+1)\left(\frac{3}{2}-\alpha\right)\right)u^2-\gamma\right)c_{ij} + \gamma d_{ij} - \alpha(1-\kappa)u^2\varphi_i(1)\varphi_j{}'(1)\Bigg]\{q_j(\tau)\} = 0 \tag{34}$$

The frequencies of the system are obtained from the non-trivial solution, and is given by the determinant of Eq. (34).

$$det\Bigg[\left(\left(\bar{\alpha}^* + \frac{\mu}{\omega}\right)\lambda_j^4 + \sigma + \lambda_j^4 - \omega^2\right)\delta_{ij} - \left(2\beta^{\frac{1}{2}}ui\omega + \gamma\right)b_{ij} + \left(\left(1-(\bar{\gamma}+1)\left(\frac{3}{2}-\alpha\right)\right)u^2-\gamma\right)c_{ij} + \gamma d_{ij}$$
$$-\beta^{\frac{1}{2}}u\varphi_i(1)\varphi_j(1)i\omega - \alpha(1-\kappa)u^2\varphi_i(1)\varphi_j{}'(1)\Bigg] = 0 \tag{35}$$

The complex eigenfrequencies ω are obtained and associated with the modal function (roots of Eq. (35)), which depend on the dimensionless flow velocity u, which increases gradual and can be solved numerically by the resulting characteristic polynomial.

The complex eigenfrequencies ω consist of two parts namely real and imaginary, respectively, $\omega = Re(\omega) + Im(\omega)$. The imaginary component of ω is the dimensionless natural frequency of the system, the real component of ω is related to the damping, the ratio of the damping being $\varsigma = -Re(\omega)/Im(\omega)$.

RESULTS AND DISCUSSION

This section initially presents the results of the stability analysis of an elastomer pipe aspirating internal fluid, these was obtained with the parameters given in Tab. 1. The results show in Tab. 2 and are compare with those reported by Rinaldi (2009), then the dynamic response of the pipe is show for a given fluid aspiration velocity.

Table 1 –Dimensionless parameters of the system under study

Parameter	Symbol	Value
Mass ratio	β	6.10x 10^{-3}
Input velocities ratio	α	0.4
Gravity ratio	γ	11.9
Angle reduction in inlet the pipe	κ	1.0
Pressures ratio	$\bar{\gamma}$	0.30
Kelvin-Voight viscoelastic coefficient	$\bar{\alpha}^*$	3.0x10^{-4}
Hysteretic damping	μ	0.03578

Stability analysis

As previously mentioned, the solution of the frequency's equation, Eq (35), was repeatedly solving using the MATLAB software varying u.The results are presented in the Argand diagram, Fig. 3, where are shows the frequencies of the first three modes. The pipe acts as a simple cantilever pipe filled with static fluid at $u = 0$; as the aspiring velocity increases, the pipe describes a damped oscillatory movement, up to a certain aspiring velocity called critical velocity the pipe loses stability describing a self-excited oscillatory movement.

For a specific aspiration velocity $u = 1$ as shown in Tab. 2, the frequencies were compared with the theory data obtained in Rinaldi (2009) showing a well agreement, also show the critical velocity u_{cr} and its corresponding critical frequency ω_{cr}. The small difference in results with Rinaldi (2009) is due to the mathematical model using, the reference considers the delay time parameter when aspirating fluid used to validate their experimental results.

Table 2 – The first three dimensionless frequencies at dimensionless velocity at $u = 1$

Mode	Value	Own results	Results from Rinaldi (2009)
First mode	$Re(\omega_1)$	5.581	5.583
	$Im(\omega_1)$	0.021	0.025
Second mode	$Re(\omega_2)$	24.196	24.192
	$Im(\omega_2)$	0.411	0.418
Third mode	$Re(\omega_3)$	63.980	63.955
	$Im(\omega_3)$	1.616	1.626
Critical values	U_{cr}	1.989	2.1
	$Re(\omega_{cr})$	5.630	5.642
	$Im(\omega_{cr})$	0.00	0.00

Figure 3 show the Argand diagram, obtained with $N = 4$, where are plotted the natural frequencies grouped together to form three curves called of modes here, moreover, as the green, purple, and blue cores curves represent the first, second, and third modes, respectively. On its right side of the figure, it shows an enlargement the curve of the first mode. Each small square on the curves represents a frequency obtained by solving Eq. (35) with velocity of integer numerical value.

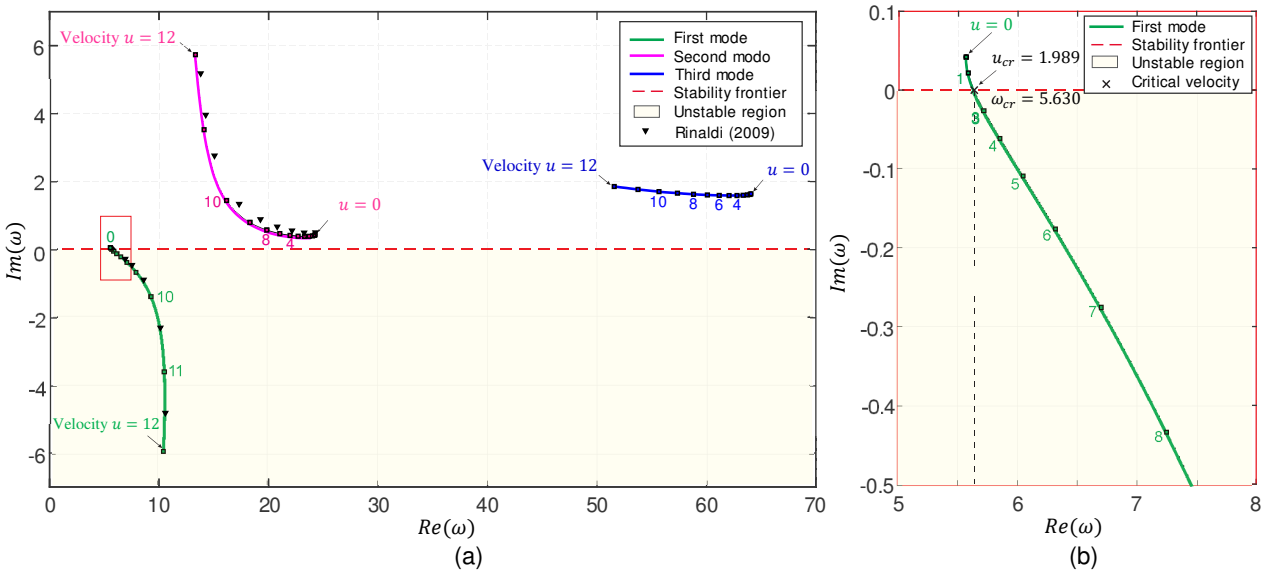

Figure 3 – Diagram de Argand: (a) Real vs. imaginary frequencies with increasing dimensional velocity; (b) magnification of the first mode.

As show in Fig, 3, the frequency with increasing of aspirating velocity u, the imaginary part, $Im(\omega)$, increase for the second and third modes, while for first mode decreases. Also, the second and third mode induce positive damping, therefore the oscillations decrease with time.

The first mode intersects the stability frontier, at point where $Im(\omega) = 0$, this frequency is called of critical frequency, $\omega_{cr} = 5.630$, corresponding at the critical velocity of aspirating, $u_{cr} = 1.989$, as seen in the magnification of the first mode on the right side of the Fig. 3. The system loses stability by flutter via Hopf bifurcation.

Figure 4 shows the real and imaginary parts of the frequency seen separately versus dimensionless fluid velocity, for a better appreciation of the oscillation and damping characteristics of the dynamics of system, with increasing the flow velocity has a stabilizing effect on the pipe in the initial stages at $u < u_{cr}$, because the imaginary component of the complex frequency grows.

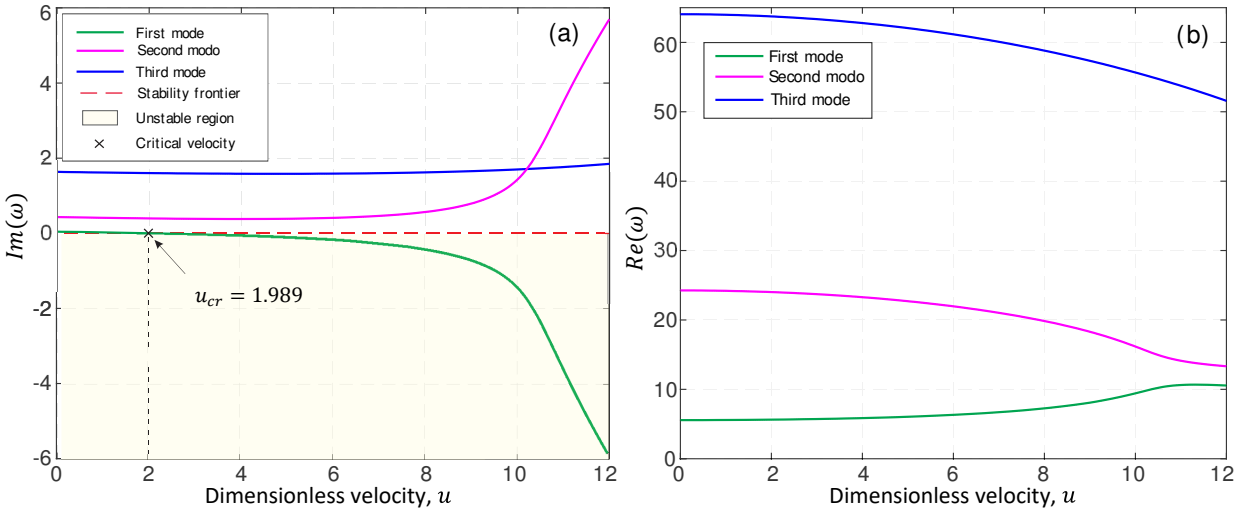

Figure 4 – Dimensionless frequency versus dimensionless aspirating velocity: (a) Imaginary component, (b) real component.

Fig. 4 (a) shows the increase in flow velocity has a stabilizing effect on the pipe in the initial stages, due to the imaginary component of the complex frequency grows in the second and third modes, but for the case the imaginary component of the first mode reaches zero at the critical flow velocity, which produces instability by flutter.

Fig. 4 (b) show the trend of the real part that represents the oscillation versus the flow velocity, at $u < 10.8$ the oscillation increases for the first mode with increased of the velocity, while for the second and three modes it decreases.

System response

The Fig. 5 present the relative amplitudes of generalized coordinates obtained by solving the Eq. (40) at $u = 1$. The first function, Fig. 5 (a), is associate with first generalized coordinate, the most relevant and associated with the first vibration mode, function quasi-periodic and with slightly amplified in time. The second function, Fig. 5(b), corresponds to the second coordinate, associated with the second vibration mode, function periodic and slight damping over time. Then, other modes of vibration, which are not plotted because they are of small amplitudes and damped.

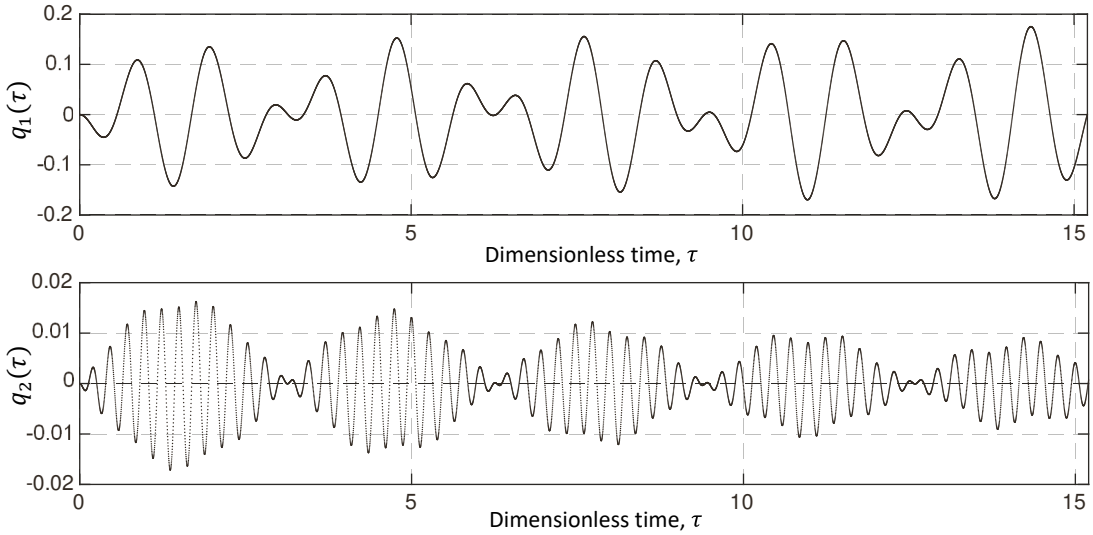

Figure 5 – The response of the (a) first and (b) second generalized coordinate at $u = 1$

The dynamic response of the pipe is presented, at aspirating velocity below the critical velocity $u = 1$, considering $N = 4$, as seen in Fig. 6, each plotted line is the configuration that the pipe adopts for a certain moment, in total 13 configurations are plotted with an interval of dimensionless time $\Delta\tau = 0.358$. The shape that the vibration of the pipe takes resembles the shape of the first mode for a cantilever beam. The shape of the modes shown agrees with the theory, at that velocity the pipe will have stable periodic oscillations with small movements.

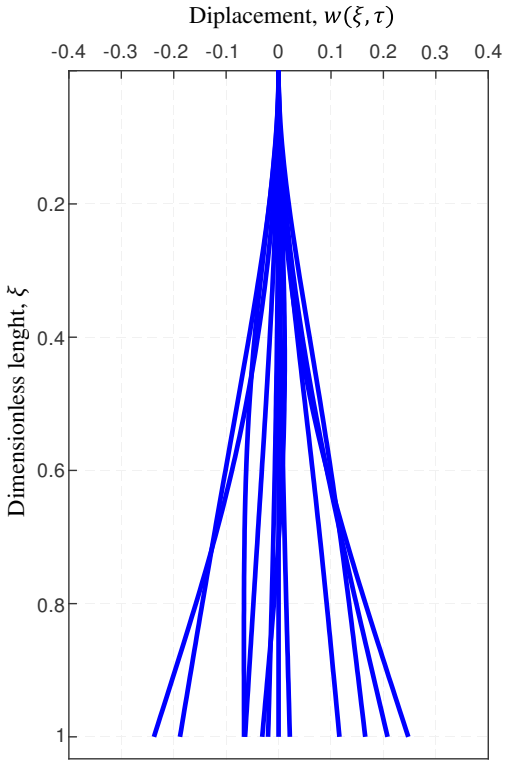

Figure 6 – The spatial response obtained with $N = 4, u = 1,\ \Delta\tau = 0.358$

CONCLUTION

In this article, the stability of a aspirating cantilever pipe was investigated, through latest analytical mode, which considered the fluid-structure dynamics of the system as a whole with approximations that shaped the model, was discretized to obtain the eigenvalues of the system, then it was plotted in the Argand diagram as a function of the aspiration velocity to analyze how the frequencies behave in their respective modes, where was it determined the critical velocity of $u_{cr} = 1.989$ at frequency $\omega_{cr} = 5.630$.

The pipe loses stability via ordinary Hopf bifurcation by flutter, which is present in the first mode as observed in Fig. 5. In addition, the motion equation of system was used to predict the dynamic behavior of the pipe, inducing a harmonic force that excites the system, first, the relative amplitude was analyzed of the first two generalized coordinates. It was observed that in the first maximum amplitudes relative of oscillations are of stable value, compared to the following, which are amortized therefore decreasing. The behavior of the pipe was presented in Fig. 4 with an aspirating velocity $u = 1$, below critical velocity, therefore the oscillations of the pipe are damping in time.

This study can be seen as another contribution to understand the meaning of pipe stability with oscillations decaying over time at stable velocity. It also contributes to the understanding of the input parameters $\alpha, \bar{\gamma}, \kappa$ that arise at the free end of the pipe, since these values can experimentally contribute to the physics of the system for its possible implementation.

REFERENCES

Giacobbi, D. B., Rinaldi, S., Semler, C., & Païdoussis, M. P. (2012). The dynamics of a cantilevered pipe aspirating fluid studied by experimental, numerical and analytical methods. *Journal of Fluids and Structures*, *30*, 73–96. https://doi.org/10.1016/j.jfluidstructs.2011.11.011

Michael P. Paidoussis. (2005). Fluid-Structure Interactions (Slender Structures and Axial Flow Vol. 1),. In *Journal of the Atomic Energy Society of Japan / Atomic Energy Society of Japan* (Second Edi, Vol. 47, Issue 3).

Minguez, M., Clergue, S., Kessel, J. Van, Bessière, L., Pattedoie, S., Renaud, M., Skledar, M., Lange, F., Miller, E., & Masterton, S. (2020). Water intake riser wir-from design to installation, an example ofcomplex structure requiring multi-disciplinary approach. *Proceedings of the Annual Offshore Technology Conference*, *2020-May*. https://doi.org/10.4043/30708-ms

Paidoussis, M. P. (1999). Aspirating pipes do not Flutter at infinitesimally small flow. *Journal of Fluids and Structures*, *13*(3), 419–425. https://doi.org/10.1006/jfls.1999.0210

Paidoussis, M. P., & Luu, T. P. (1985). Dynamics of a Pipe Aspirating Fluid Such as Might be Used in Ocean Mining. *Journal of Energy Resources Technology*, *107*(2), 250–255. https://doi.org/10.1115/1.3231185

Paidoussis, Mary P., Semler, C., & Wadham-Gagnon, M. (2005). A reappraisal of why aspirating pipes do not flutter at infinitesimal flow. *Journal of Fluids and Structures*, *20*(1), 147–156. https://doi.org/10.1016/J.JFLUIDSTRUCTS.2004.09.004

Rinaldi, S. (2009). *Experiments on the dynamics of cantilevered pipes subjected to internal and/or external axial flow*. McGill University.

Rodrigo Klim. (2021, February 16). *The advantages of building a pilot ocean thermal energy conversion (OTEC) plant in Brazil*. https://www.linkedin.com/pulse/advantages-building-pilot-ocean-thermal-energy-conversion-klim/

RESPONSIBILITY NOTICE

The authors are the only responsible for the printed material included in this paper.